

Flux-Switching Floquet Engineering

Ian Emmanuel Powell and Louis Buchalter

Physics Department, California Polytechnic State University San Luis Obispo California.

(Dated: September 9, 2025)

We present an analysis of a square-lattice Harper-Hofstadter model with a periodically varying magnetic flux with time. By switching the dimensionless flux per plaquette between a set of values $\{p_j/q_j\}$ the Floquet quasienergy spectrum is folded into $Q = \text{lcm}\{q_j\}$ bands. We determine closed-form analytical solutions for the quasienergy spectrum and Chern numbers for the $-1/2 \rightarrow 1/2$ flux switching case, as well as the Rudner-Lindner-Berg-Levin (RLBL) winding invariants W numerically, and construct the corresponding topological phase diagram for arbitrary driving period. We find that generic flux-switching drives feature interlaced Hofstadter butterfly quasienergy spectra, and the gaps in the spectrum may be labeled according to a Diophantine equation which relates the quasienergy gap index to the fluxes attained in the drive and their associated per-step windings.

I. INTRODUCTION

Periodically driven, or Floquet, quantum matter provides a powerful arena in which band structures, symmetries and even dimensionality can be tuned on demand [1–3]. These periodically driven systems can display a wide variety of rich phenomena such as dynamical localization [4], coherent destruction of tunneling [5], and the emergence of anomalous topological phases whose bulk Chern numbers vanish even as robust chiral edge modes persist [6–8]. Experimental protocols have successfully implemented periodic driving to realize the novel non-equilibrium physics involved: photonic waveguide arrays with helically modulated couplings have been used to realize topological phases [9], and ultracold atoms in shaken optical lattices have been used to realize the Floquet Haldane model [10]. More recently, signatures of the so-called Floquet anomalous topological insulators have been inferred via edge transport imaging [11], the light-induced anomalous Hall effect has been directly measured in graphene [12], and higher-order Floquet topological states have been realized in three-dimensional acoustic lattices [13].

In this manuscript, we investigate a periodically driven Harper–Hofstadter model in which the dimensionless flux per plaquette is toggled between distinct rational values over each driving period. This time-periodic flux modulation fragments the quasienergy spectrum into a structured set of magnetic subbands, leading to a vast nontrivial topological phase diagram in which quasienergy gaps are labeled by their Rudner-Lindner-Berg-Levin (RLBL) winding invariants W , including “anomalous” windings in which chiral edge modes propagate through the Floquet zone edge. We further show that the global organization of gaps follows a compact Diophantine congruence that links each gap label to step-resolved winding contributions. Although our analysis primarily focuses on noninteracting charged fermions on a square lattice, the same Floquet framework applies directly to bosonic cold-atom setups: by modulating Raman-laser detunings and intensities in time, one can realize our flux-switching protocol on existing experimental platforms [14, 15].

II. THEORY

We consider a model of free electrons on a square lattice that are subject to a periodic flux switching routine in which the dimensionless flux per plaquette switches between rational $\alpha = p/q$ at regular intervals in time. For example, for two-flux routines, the electrons are subject to two distinct magnetic fields that are perpendicular to the plane of the lattice— \mathbf{B}_1 , with associated dimensionless flux per plaquette α_1 , for a time T_1 , followed by a magnetic field \mathbf{B}_2 , with associated dimensionless flux per plaquette α_2 , for a time T_2 , and so on. The time evolution operator for one full period of the drive is given in natural units as

$$U(T + t_0, t_0) = \mathcal{T} \exp \left[-i \int_{t_0}^{t_0+T} H(t) dt \right], \quad (1)$$

where T is the period of the drive, and \mathcal{T} denotes time-ordering. Given a sequence of flux quenches with L distinct steps, i.e. for the case where the magnetic flux discontinuously jumps between different values L times, and taking the reference time $t_0 = 0$, eq. (1) factorizes to the time-ordered product of constituent unitaries

$$U(T) = \prod_{j=1}^L \exp[-i H_j T_j] = \exp[-i H_F T], \quad (2)$$

where $T = \sum_j T_j$, H_j is the Hamiltonian that describes the electrons during the j^{th} step of the drive, and H_F is the effective Floquet Hamiltonian—the generator of the stroboscopic dynamics. Given the definition of H_F featured in Eq. (2) the eigenvalues, or “quasienergies,” of H_F are defined modulo $2\pi/T$.

The constituent Hamiltonians, H_j , in Eq. (2) describe non-interacting electrons in the presence of an external magnetic field, or non-interacting bosons in the presence of a synthetic gauge field arising from laser induced Raman-assisted tunneling. They read

$$H_j = - \sum_{\mathbf{r}, \mathbf{r}'} t_{\mathbf{r}, \mathbf{r}'} e^{-i\phi_{j, \mathbf{r}, \mathbf{r}'}} c_{\mathbf{r}}^\dagger c_{\mathbf{r}'} + \text{h.c.}, \quad (3)$$

where $t_{\mathbf{r}, \mathbf{r}'}$ is the hopping integral from site \mathbf{r} to \mathbf{r}' , $c_{\mathbf{r}}^\dagger$ and $c_{\mathbf{r}'}$ are the electron (boson) particle creation and an-

annihilation operators at the sites \mathbf{r} and \mathbf{r}' respectively, spin indices have been suppressed, and $\phi_{j,\mathbf{r},\mathbf{r}'}$ is the Peierls phase acquired by the hopping of particles in the presence of the magnetic field (synthetic gauge field) $\phi_{j,\mathbf{r},\mathbf{r}'} = \frac{e}{\hbar} \int_{\mathbf{r}}^{\mathbf{r}'} \mathbf{A}_j(\mathbf{l}) \cdot d\mathbf{l}$. Upon selecting the Landau gauge $\mathbf{A}_j = (-B_j y, 0, 0)$ and including nearest and next-nearest neighbor hopping terms, the Hamiltonians are explicitly written as

$$H_j = H_j^{\text{NN}} + H_j^{\text{NNN}}, \quad (4)$$

with

$$H_j^{\text{NN}} = -t \sum_{m,n} \left[e^{-i2\pi\alpha_j n} c_{m+1,n}^\dagger c_{m,n} + c_{m,n+1}^\dagger c_{m,n} \right] + \text{h.c.}, \quad (5)$$

$$H_j^{\text{NNN}} = -t' \sum_{m,n} \left[e^{-i2\pi\alpha_j(n+1/2)} c_{m+1,n+1}^\dagger c_{m,n} + e^{-i2\pi\alpha_j(n-1/2)} c_{m+1,n-1}^\dagger c_{m,n} \right] + \text{h.c.}, \quad (6)$$

where $\alpha_j = p_j/q_j$ (with coprime p_j and q_j) is the reduced dimensionless flux per plaquette in step j , and the lattice coordinates on the square lattice are given via $\mathbf{r} = ma \hat{\mathbf{x}} + na \hat{\mathbf{y}}$ with lattice constant a .

For each step in the time evolution of the system subject to a sequence of fluxes $\{\alpha_j\} = \{p_j/q_j\}$ the lattice magnetic translations T_x, T_y satisfy Zak's algebra [16–18]

$$T_x T_y = e^{i2\pi\alpha_j} T_y T_x, \quad \alpha_j = \frac{p_j}{q_j}. \quad (7)$$

Hence $[T_x^\ell, T_y^h] = 0$ if $e^{i2\pi\alpha_j \ell h} = 1$. Consequently, the minimal area supercell compatible with all steps in the drive must have area ℓh (in units of a^2) that is an integer multiple of the least common multiple of the set of all $\{q_i\}$ —i.e the minimal cell has area $Q \equiv \text{lcm}\{q_j\}$.

Selecting $(\ell, h) = (1, Q)$, the magnetic translations T_x and T_y^Q commute with each H_j (and thus with each U_j). This choice defines a magnetic unit cell that is Q times longer along y . With this choice one has, for every step j ,

$$T_y^Q U_j (T_y^Q)^\dagger = U_j, \quad [U_j, T_x] = 0. \quad (8)$$

Inserting $T_y^Q (T_y^Q)^\dagger$ between steps in the Floquet product straightforwardly yields

$$[T_y^Q, U(T)] = 0, \quad [T_x, U(T)] = 0. \quad (9)$$

We therefore simultaneously diagonalize $U(T)$, T_x , and T_y^Q . The quasienergy spectrum splits into Q magnetic subbands, and Bloch's theorem holds in the reduced (magnetic) Brillouin zone (RBZ)

$$k_x \in \left(-\frac{\pi}{a}, \frac{\pi}{a}\right], \quad k_y \in \left(-\frac{\pi}{Qa}, \frac{\pi}{Qa}\right]. \quad (10)$$

Before we proceed, a couple of remarks regarding time-varying flux are in order. First, it should be noted that introducing finite, continuous ramps of duration τ between the piecewise steps in Eq. (2) formally breaks the exact magnetic translation symmetry of the ideal case of a series of quenches. However, provided $\tau/T \ll 1$ these ramps do not close the primary quasienergy gaps, so all associated topological features remain intact. Consequently, although we omit the ramping terms from our main analysis, our results remain valid in the appropriate small-ramp-time limit where primary gaps are not destroyed. We demonstrate the effect of including ramping terms for a model driven between $-1/2$ and $1/2$ flux in Appendix A. Second, by Faraday's law, any temporal change in flux induces an electric field in electronic systems. In cold-atom Raman-assisted-tunneling implementations the time varying gauge field manifests as an analogous synthetic electric field [19]. In either realization identical stroboscopic Floquet-Bloch Hamiltonian matrices are produced.

In terms of experimental realizability, Moiré heterostructures (e.g., twisted bilayer graphene) may host a large flux per unit cell, but to realize access the high-frequency (and intermediate frequency) regimes, one must alternate the magnetic flux at ultrafast scales set by the band gap widths. With $t \sim 1$ meV and our dimensionless choice for the high frequency cutoff $T \sim 1$, the drive frequency is $\omega \sim t/\hbar \approx 1.5 \times 10^{12} \text{ s}^{-1}$. By contrast, Raman-assisted tunneling in cold atom systems can realize uniform synthetic flux with α continuously tunable over $[0, 1)$ [14, 15], and for typical parameters $t/\hbar \sim .1 - 1$ kHz, kHz drive frequencies correspond to $T \sim \mathcal{O}(1)$ in our dimensionless units—thus the high and intermediate frequency regimes are much more accessible. Furthermore, higher frequency driving leads to exponentially long prethermal plateaus [20], making direct measurements more feasible. These considerations make cold-atom platforms the most natural testbed for our flux-switching protocol.

A. Topology and Chiral Edge States

For this $2 + 1$ dimensional time periodic system the Floquet-Bloch time evolution operator, $U(k_x, k_y, t)$, defines a map from the three-torus ($\text{RBZ} \times S^1$) to the unitary group of $Q \times Q$ matrices, $U(Q)$, where again $Q = \text{lcm}\{q_j\}$. This map carries a winding known as the RLBL winding, W_ε , which accurately predicts the number of chiral edge modes propagating through each gap at ε in the quasienergy spectrum [7]. The first Chern number of the occupied bundle, C , which is featured in the familiar quantization of the integer quantum Hall conductivity [21], is the total Berry flux through the RBZ bundle; it accurately predicts the number of chiral edge modes propagating through each gap provided no “anomalous” modes cross the Floquet boundary at $\varepsilon = \pm \frac{\pi}{T}$. As a rule of thumb, when each instantaneous Hamiltonian's operator norm satisfies $\|H_j\| T < \pi$, no anomalous winding

occurs and the Chern numbers of the quasienergy bands suffice to fully characterize the topology. On the other hand, When $\|H_j\|T \geq \pi$, anomalous modes at $\varepsilon = \pm\pi/T$ may appear, and one must compute the RLBL winding, W_ε , to obtain the correct edge-mode count.

To define W_ε we proceed in the usual way by defining the bulk time evolution operator $U(\mathbf{k}, t) = \mathcal{T} \exp[-i \int_0^t H(\mathbf{k}, t') dt']$, and the branch cut-specified Floquet Hamiltonian by

$$U(\mathbf{k}, T) = e^{-iT H_F^{(\varepsilon)}(\mathbf{k})}, \quad H_F^{(\varepsilon)}(\mathbf{k}) = \frac{i}{T} \log_{-\varepsilon T} U(\mathbf{k}, T), \quad (11)$$

where $\log_{-\varepsilon T}$ denotes the logarithm with the branch cut located at $e^{-i\varepsilon T}$ -i.e. $\log_{-\varepsilon T}(e^{i\phi}) = i\phi$ for $-\varepsilon T - 2\pi < \phi \leq -\varepsilon T$. The periodized evolution is then defined as the unitary

$$V_\varepsilon(\mathbf{k}, t) = U(\mathbf{k}, t) e^{+it H_F^{(\varepsilon)}(\mathbf{k})}, \quad (12)$$

which is smooth on the three-torus $\mathbb{T}^3 = \text{RBZ} \times S^1$ and satisfies $V_\varepsilon(\mathbf{k}, 0) = V_\varepsilon(\mathbf{k}, T) = \mathbb{1}$. The RLBL winding of the gap at ε is [22]

$$W_\varepsilon = \frac{1}{24\pi^2} \int_{\text{RBZ} \times S^1} \text{Tr} [(V_\varepsilon^{-1} dV_\varepsilon)^3], \quad (13)$$

which equals the net number of chiral edge modes crossing the quasienergy gap at ε . If $\{\varepsilon_n\}$ lists the gaps in order (including that at the bottom boundary of the principal Floquet zone, $-\pi/T$), the band Chern numbers $\{C_n\}$ satisfy the telescoping relations [7]

$$C_n = W_{\varepsilon_{n+1}} - W_{\varepsilon_n}, \quad \sum_n C_n = 0, \quad (14)$$

To evaluate W_ε one can either count the number of chiral edge modes propagating through the π/T gap in the principal Floquet zone, implement the Floquet-Středa formula [23], or one may numerically evaluate the bulk winding of the mapping to U via a cubic grid of k_x, k_y, t values, Λ . We implement all three methods in this manuscript; but in the following section we elect to numerically compute W_ε . To this end, we implement the formula of Morikawa and Suzuki [24] which we briefly review here. The derivatives in Eq. (13) are replaced via

$$V_\varepsilon^{-1} \partial_\mu V_\varepsilon \rightarrow \frac{1}{4} \Omega_\varepsilon(\mathbf{x}, \mathbf{y}), \quad (15)$$

where $\mathbf{x} = (k_x, k_y, t) \in \Lambda$ and

$$\begin{aligned} \Omega_\varepsilon(\mathbf{x}, \mu) = & V_\varepsilon^{-1}(\mathbf{x}) \left[V_\varepsilon(\mathbf{x} + \hat{\mu}) - V_\varepsilon(\mathbf{x} - \hat{\mu}) \right. \\ & - \frac{1}{6} \{ V_\varepsilon(\mathbf{x} + 2\hat{\mu}) - 2V_\varepsilon(\mathbf{x} + \hat{\mu}) \\ & \left. + 2V_\varepsilon(\mathbf{x} - \hat{\mu}) - V_\varepsilon(\mathbf{x} - 2\hat{\mu}) \} \right] - \text{H.c.} \end{aligned} \quad (16)$$

with $\mu = k_x, k_y, t$. The RLBL winding (Eq. (13)), is calculated on the discrete grid as approximately

$$\begin{aligned} W_\varepsilon \approx & \frac{1}{4^3 24 \pi^2} \sum_{\mathbf{x} \in \Lambda} \sum_{\mu, \nu, \rho} \epsilon_{\mu\nu\rho} \\ & \times \text{Tr} [\Omega_\varepsilon(\mathbf{x}, \mu) \Omega_\varepsilon(\mathbf{x}, \nu) \Omega_\varepsilon(\mathbf{x}, \rho)]. \end{aligned} \quad (17)$$

All calculations of W_ε are performed on a $91 \times 91 \times 51$ grid when using the above expression.

B. $(-1/2 \rightarrow 1/2)$ Flux Switching

We begin by considering the simplest possible nontrivial two-step protocol where the flux is switched between $\alpha = -1/2$ and $\alpha = +1/2$ with a nonzero NNN hopping integral. This drive admits a closed-form solution to the quasienergies in momentum space as well as the quasienergy band Chern numbers provided they are well separated from one another. Denoting the dwell times in the $-1/2$ and $1/2$ flux steps by T_1 and T_2 , the single-particle Bloch Hamiltonians in the y -even-odd sublattice basis are obtained via the appropriate Fourier transformations of Eq. (4) as

$$\begin{aligned} H_{\pm 1/2}(\mathbf{k}) &= -2t \mathbf{h}_{\pm 1/2}(\mathbf{k}) \cdot \boldsymbol{\sigma}, \\ \mathbf{h}_{\pm 1/2}(\mathbf{k}) &= (\cos k_y, \mp 2\tilde{t} \sin k_x \sin k_y, \cos k_x), \end{aligned} \quad (18)$$

where $\tilde{t} = t'/t$. Each step implements an $\text{SU}(2)$ rotation:

$$U_{-1/2}(\mathbf{k}) = \exp[i \theta_1(\mathbf{k}) \hat{\mathbf{n}}_-(\mathbf{k}) \cdot \boldsymbol{\sigma}], \quad \theta_1 = 2t T_1 |\mathbf{h}_\mathbf{k}|, \quad (19)$$

$$U_{+1/2}(\mathbf{k}) = \exp[i \theta_2(\mathbf{k}) \hat{\mathbf{n}}_+(\mathbf{k}) \cdot \boldsymbol{\sigma}], \quad \theta_2 = 2t T_2 |\mathbf{h}_\mathbf{k}|, \quad (20)$$

where

$$\hat{\mathbf{n}}_\pm(\mathbf{k}) = \frac{\mathbf{h}_{\pm 1/2}(\mathbf{k})}{|\mathbf{h}_\mathbf{k}|}, \quad (21)$$

and

$$|\mathbf{h}_\mathbf{k}| = \sqrt{\cos^2 k_y + 4\tilde{t}^2 \sin^2 k_x \sin^2 k_y + \cos^2 k_x}. \quad (22)$$

Thus, the one-period Bloch-Floquet operator can be represented as a single equivalent $\text{SU}(2)$ rotation

$$U(\mathbf{k}, T) = U_{+1/2}(\mathbf{k}) U_{-1/2}(\mathbf{k}) = \exp[i \Theta(\mathbf{k}) \hat{\mathbf{n}}_F(\mathbf{k}) \cdot \boldsymbol{\sigma}], \quad (23)$$

with

$$\cos \Theta(\mathbf{k}) = \cos \theta_1 \cos \theta_2 - (\hat{\mathbf{n}}_+ \cdot \hat{\mathbf{n}}_-) \sin \theta_1 \sin \theta_2, \quad (24)$$

$$\begin{aligned} \hat{\mathbf{n}}_F(\mathbf{k}) \sin \Theta(\mathbf{k}) = & \hat{\mathbf{n}}_- \sin \theta_1 \cos \theta_2 + \hat{\mathbf{n}}_+ \sin \theta_2 \cos \theta_1 \\ & + (\hat{\mathbf{n}}_- \times \hat{\mathbf{n}}_+) \sin \theta_1 \sin \theta_2. \end{aligned} \quad (25)$$

The quasienergies are then

$$\varepsilon_\pm(\mathbf{k}) = \pm \frac{\Theta(\mathbf{k})}{T} + \frac{2\pi m}{T}, \quad m \in \mathbb{Z}, \quad (26)$$

where $T = T_1 + T_2$ and $\Theta(\mathbf{k})$ is determined from the principal value of Eq. (24). The inverse cosine operation is defined modulo 2π ; hence, the integer $m \in \mathbb{Z}$ in Eq.

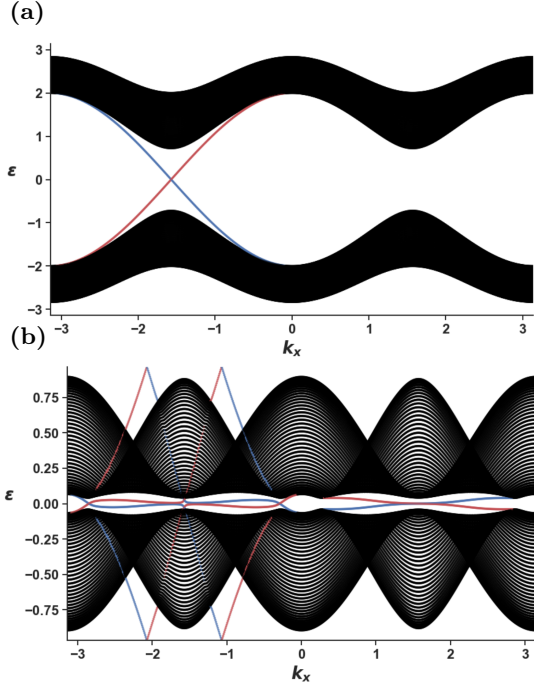


FIG. 1. Floquet strip spectra plotted in the principal Floquet zone, $\varepsilon \in (-\pi/T, \pi/T]$, for a cylinder of height $N_y = 90$ under the $\pm 1/2$ driving protocol and the associated topological phase diagrams. In the quasienergy plots the vertical axes are listed in units of t , the horizontal axes are in units of inverse lattice spacing, a^{-1} , and the red (blue) curves denote states that are localized to the top (bottom) of the cylinder. (a) $T_2 = 0.8$, $1/2$ flux dominates and the Chern numbers of the bottom and top bands mimic the static π -flux Harper model $(C_b, C_t) = (1, -1)$. (b) $T_2 = 3.05$, a band touching event leads to RLBL invariants $W_\pi = 2$, $W_0 = 1$ and hence a Chern inversion $(C_b, C_t) = (-1, 1)$.

(26) accounts for the infinitely many equivalent branches in the quasienergy spectrum—an expected feature in any Floquet system. We plot the quasienergy spectrum for the $\pm 1/2$ driving protocol on a cylindrical strip geometry for several values of T_1 and $T_2 = 0.2$ along with the Chern and RLBL winding numbers W_0 and W_π in Fig. 2. We explicitly demonstrate the robustness of the flipped topological phase to finite flux ramps in Appendix A.

Given that there are two quasienergy bands in the principal zone for the $-1/2 \rightarrow 1/2$ drive it is possible to derive an expression for the Chern numbers analytically. One finds after an explicit evaluation (see Appendix B) that the Chern number of the “bottom” band in the principal Floquet zone reduces to the simple form when the gaps at 0 and π/T are open

$$C_b = \text{sgn}[\sin(4t'(T_2 - T_1))]. \quad (27)$$

Equation (27) agrees with the results plotted in Fig. 1 by employing Eq. (14). For $T_1 = 0.2$ and $1.4 \lesssim T_2 < 2$ $W_0 - W_\pi = C_b = 1$, whereas for the anomalous window where $T_2 \sim 3$ we have that $W_0 - W_\pi = C_b = -1$. When $T_1 = T_2$, or when $t' = 0$, the drive is invariant under time reversal symmetry and the bands never separate from one another. The full Chern phase diagram is plotted in Fig.

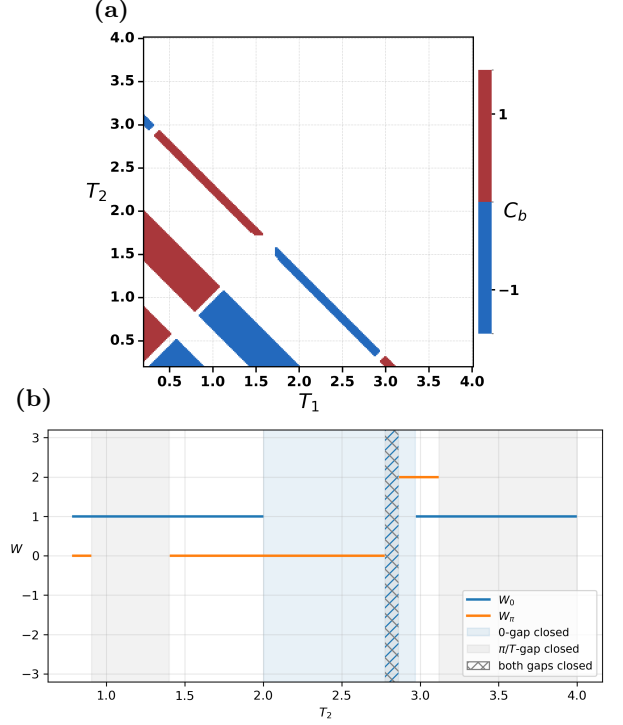


FIG. 2. (a) Chern number of the bottom band in the principal Floquet zone, C_b , as predicted by Eq. (27) plotted versus dwell times T_1 and T_2 with $t' = 0.3t$. White areas are regions where the two bands are not well separated, and the origin corresponds to $T_1 = T_2 = 0.2$. Topological phases with nonzero W_π occur for small windows of T_1, T_2 values: $T_1 \sim .2$, $T_2 \sim 3$, and $T_1 \sim 3$, $T_2 \sim .2$. (b) W_π and W_0 calculated using Eq. (17) plotted as a function of T_2 with $T_1 = 0.2$; values deviate from $W = 0, 1, 2$ by a maximum of $\pm 10^{-3}$.

2. We note that the flipped topological phases occupy larger regions in $T_1 - T_2$ space when the NNN hopping is increased relative to the NN hopping, i.e. when \tilde{t} is increased; and, in fact, for $\tilde{t} < 0.25$ the flipped Chern phase cannot be realized at all.

III. GENERAL DRIVES

Now we consider the more general case of flux switching routines in which the flux switches between arbitrary α_j values. For the general case the Bulk Floquet operator is the time-ordered product

$$U(\mathbf{k}, T) = \prod_j U_j(\mathbf{k}, T_j) \quad (28)$$

with the constituent bulk unitaries determined as

$$U_j(\mathbf{k}, T_j) = \exp[-iH_j(\mathbf{k})T_j], \quad (29)$$

and the effective Floquet bulk Hamiltonian defined via

$$U(\mathbf{k}, T) = \exp[-iH_F(\mathbf{k})T]. \quad (30)$$

The bulk Hamiltonian for the j^{th} step is defined on the Q -folded RBZ by performing the appropriate Fourier transformations of Eq. (4)

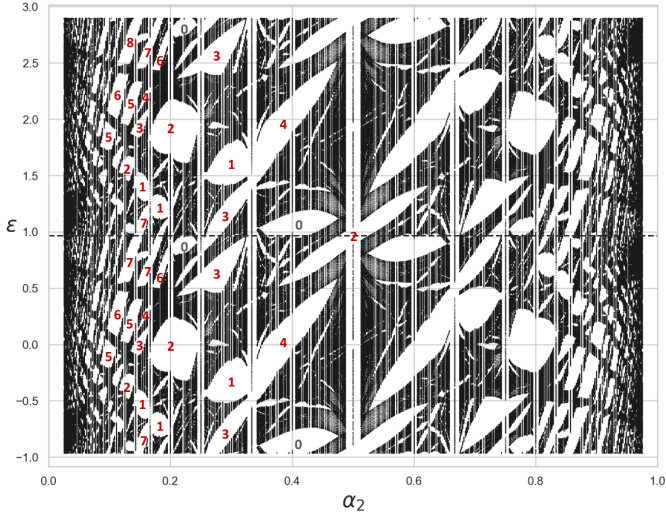


FIG. 3. Butterfly quasienergy spectrum for $\alpha_1 = -1/2$, $T_1 = 0.2$, $T_2 = 3.05$, $t' = 0.3$ plotted for two adjacent Floquet zones. The dashed horizontal line indicates the top edge of the principal Floquet zone $\varepsilon = \pi/T$, and α_2 values are selected from the set of all unique reduced fractions $0 < p_2/q_2 < 1$ with $q_{2,\max} = 40$. W invariants are listed for a selection of the main gaps in red text. We verify agreement between the Floquet–Středa equation (Eq. (33)), the approximate Suzuki–Morikawa expression (Eq. (17)), and the number of chiral edge modes in each gap.

$$\begin{aligned}
 H_j(\mathbf{k}) &= -2tC_0 - t(e^{-ik_y}S^\dagger + e^{ik_y}S) \\
 &\quad - 2t'(e^{ik_y}SC_{1/2} + e^{-ik_y}S^\dagger C_{-1/2}); \\
 C_\delta &= \text{diag}\left(\cos[k_x - 2\pi\alpha_j(m + \delta)]\right)_{m=0}^{Q-1}, \\
 S_{mn} &= \delta_{m,n+1 \pmod{Q}}, \quad S_{mn}^\dagger = \delta_{m,n-1 \pmod{Q}}.
 \end{aligned} \tag{31}$$

A complete “butterfly” quasienergy spectrum may be obtained by diagonalizing Eq. (28) and varying the values of each α_j . Given L distinct flux steps at fixed values of $\{T_j\}$, it is an $L+1$ dimensional object with the quasienergy gaps forming empty chambers in the space. We plot a slice of the quasienergy butterfly spectrum for $\alpha_1 = -1/2$, $T_1 = 0.2$, and $T_2 = 3.05$ by varying α_2 and diagonalizing $U(\mathbf{k}, T)$ in Fig. 3. Notably, the gap centered at $\alpha_2 = 1/2$, $\varepsilon = \pi/T$ carries $W = 2$ for a range of nearby fluxes regardless of whether the gap straddles the Floquet boundary (and hence carries the winding labeled W_π) or not.

In the static Harper–Hofstadter model, the Středa formula [25] may be used to relate the rate of change of occupied states with magnetic flux to the sum of the Chern numbers of the occupied bands. Recently, the Floquet analogue of the Středa formula was developed [23] which we may use with particular benefit for our purposes here. The windings through a given gap at quasienergy $\varepsilon = \mu$ for a general driven model are partitioned into normal (N) and anomalous (A) contributions

$$W(\mu) = W^N(\mu) + W^A \tag{32}$$

where

$$W^N(\mu) = \frac{\partial N_{\text{eff}}(\mu)}{\partial \alpha}, \quad W^A = \frac{1}{\omega} \frac{\partial \text{Tr}[H_F]}{\partial \alpha}. \tag{33}$$

The normal contribution to the winding quantifies the spectral flow between the edge and the bulk of the system—it is essentially equivalent to the Středa response of a static system. On the other hand, the anomalous contribution may possibly be understood as a quantized energy flow between the system and the driving field(s) [23]. In the original construction of this expression α is treated as an artificial flux which is threaded through the lattice—it perturbs the base-model under consideration, and the response of the system to this magnetic flux quantifies the winding through a given gap. Above, $\omega = 2\pi/T$ is the frequency of the drive, and $N_{\text{eff}}(\mu)$ is the number of states counted in the “natural” Floquet zone (NFZ) defined in Ref. [26] up to a threshold chemical potential, μ . The NFZ is the width $2\pi/T$ interval in quasienergy whose band indices, n , are fixed by the unique condition that the sum of the quasienergies equals the time-averaged trace of the full time-dependent Hamiltonian over a period $\sum_n \varepsilon_n(\mathbf{k}) = \frac{1}{T} \int_0^T \text{Tr}[H(\mathbf{k}, t)] dt$. With this understanding, Eq.s (32), (33) produce results consistent with Eq. (17) as well as the visual count of chiral edge modes spanning each gap. We note that choosing the naive principal Floquet zone is entirely sufficient for unambiguous band labeling in the high frequency regime.

For the L -step arbitrary flux-switching drive Eq. (33) may be expressed as

$$W^N(\mu) = \mathbf{u} \cdot \nabla_{\boldsymbol{\alpha}} N_{\text{eff}}(\mu) \tag{34}$$

and

$$W^A = \frac{1}{\omega} \mathbf{u} \cdot \nabla_{\boldsymbol{\alpha}} \text{Tr}[H_F], \tag{35}$$

where the vector $\mathbf{u} = (1, 1, \dots, 1)$ has length L , and $\boldsymbol{\alpha} = (\alpha_1, \alpha_2, \dots, \alpha_L)$ is the vector of dimensionless flux values attained in a period.

Let us first consider the anomalous contribution to the winding Eq. (35). Following a similar argument to that illustrated in [27] we use the determinant identities $\det(\exp[A]) = \exp(\text{Tr}[A])$, $\det(AB) = \det(A)\det(B)$, along with Eq. (2) to write

$$\begin{aligned}
 \det(U(T)) &= \exp(-iT \text{Tr}[H_F]) \\
 &= \exp\left(-i \sum_{j=1}^L T_j \text{Tr}[H_j]\right),
 \end{aligned} \tag{36}$$

hence

$$\text{Tr}[H_F] = \sum_{j=1}^L \frac{T_j}{T} \text{Tr}[H_j] + m(\boldsymbol{\alpha})\omega, \tag{37}$$

where $m(\boldsymbol{\alpha})$ is an integer that must be included due to the mod ambiguity of the equality of complex exponentials in

Eq. (36)–it acts as a branch cut index. Putting together Eq.s (35), (37) we have

$$W^A = \sum_{j=1}^L \frac{T_j}{2\pi} \partial_{\alpha_j} \text{Tr}[H_j] + \mathbf{u} \cdot \nabla_{\alpha} m(\alpha). \quad (38)$$

For the Harper-Hofstadter model in question, the trace of all constituent Hamiltonians in the time evolution, with or without ramping present, vanishes—that is $\text{Tr}[H_j] = 0$ for all α_j . In this case, Eq. (38) reduces to

$$W^A = \mathbf{u} \cdot \nabla_{\alpha} m(\alpha). \quad (39)$$

Given the toroidal topology of the lattice, the differentiation with respect to α is understood to be a finite difference due to the quantization of the magnetic monopole charge. The net anomalous winding through each gap is hence interpreted as the cumulative wrapping of quasienergies about the Floquet boundary at $\varepsilon = \pm\pi/T$ as each flux in the driving routine is varied—a direct generalization of the result obtained in [27].

As for the normal contribution to the total winding, Eq. (34) may be integrated to yield the Diophantine equation

$$N_{\text{eff}}(\mu) = s(\mu) + \sum_{j=1}^L W_j^N(\mu) \alpha_j, \quad (40)$$

where $W_j^N(\mu) = \partial_{\alpha_j} N_{\text{eff}}(\mu)$ is the integer contribution of the j^{th} step in the drive to the total normal winding of the gap. Defining the effective number of states per reduced magnetic unit cell $N_{\text{eff}} = [r \pmod{Q}]/Q$ we yield the Wannier-like equation [28]

$$r \pmod{Q} = Qs(\mu) + \sum_{j=1}^L W_j^N(\mu) \tilde{p}_j, \quad (41)$$

or, equivalently

$$r \pmod{Q} = \sum_{j=1}^L W_j^N(\mu) \tilde{p}_j \pmod{Q}, \quad (42)$$

where $\tilde{p}_j = Q p_j / q_j$. In the above expressions r is taken mod Q to ensure applicability in the extended Floquet zone scheme, but when working in the natural Floquet zone there is no ambiguity, so one may discard the mod Q and attribute to each gap a definite r value, with the understanding that the top and bottom gaps are labeled the same, $r = Q \pmod{Q} = 0$. We remark that this Diophantine equation is very similar in form to that which one would obtain when investigating higher-dimensional Harper-Hofstadter models [29, 30], but the integers here are related to a temporal contribution to a single net winding in a gap, whereas in higher dimensions the integer windings are interpreted as a Hall response associated with each distinct plane that comprises the lattice. We thus see that the gaps in the quasienergy spectrum may

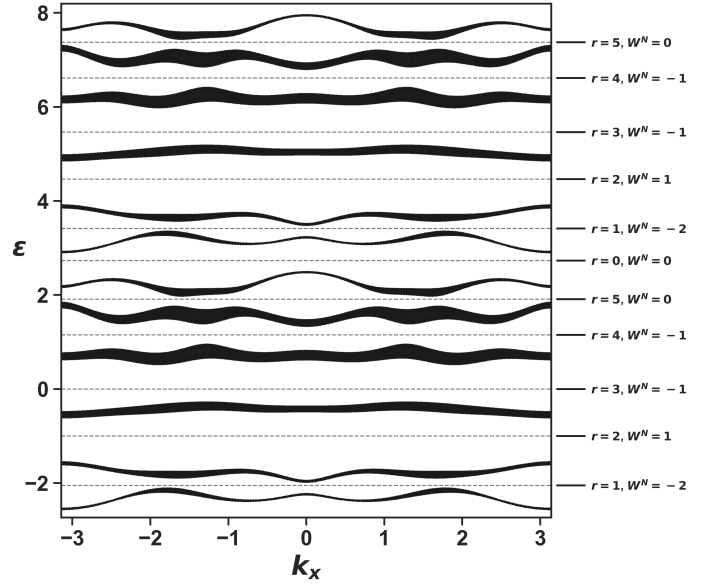


FIG. 4. Bulk quasienergy spectrum for the $\mathbf{T} = (0.5, 0.5, 0.15)$, $\alpha = (-\frac{2}{3}, -\frac{1}{2}, \frac{1}{3})$ drive with gap labels in two adjacent Floquet zones. Within each gap the per-step windings and the corresponding Diophantine equation are explicitly listed in Table II

be labeled according to the per-step windings, $W_j^N(\mu)$ accrued in each cycle, whereas the anomalous contribution to the net winding is not involved in the gap labeling. We list solutions to Eq. (42) for a three-flux drive for two different sets of dwell times $\mathbf{T} = (T_1, T_2, T_3)$ in Tables I and II. We plot the bulk band dispersion of the situation illustrated in Table I, flattened along k_y , and include gap labeling in Fig. 4.

Table I.

W^N	W_1^N	W_2^N	W_3^N	Σ	$(\Sigma \pmod{Q}) = r$
0	0	1	-1	-5	1
1	0	0	1	2	2
-1	0	-1	0	3	3
-1	0	0	-1	-2	4
0	0	-1	1	5	5

$\mathbf{T} = (0.2, 0.6, 0.4)$, $\alpha = (-\frac{2}{3}, -\frac{1}{2}, \frac{1}{3})$. $Q = \text{lcm}(3, 2, 3) = 6$;
 $(\tilde{p}_1, \tilde{p}_2, \tilde{p}_3) = (-4, -3, 2)$. $r = \sum_j W_j^N \tilde{p}_j \pmod{Q}$;
 $\Sigma = -4W_1^N - 3W_2^N + 2W_3^N$.

Table II.

W^N	W_1^N	W_2^N	W_3^N	Σ	$(\Sigma \pmod{Q}) = r$
-2	-1	-1	0	7	1
1	1	0	0	-4	2
-1	0	-1	0	3	3
-1	-1	0	0	4	4
0	1	-1	0	-1	5

$\mathbf{T} = (0.5, 0.5, 0.15)$, $\alpha = (-\frac{2}{3}, -\frac{1}{2}, \frac{1}{3})$. $Q = \text{lcm}(3, 2, 3) = 6$;
 $(\tilde{p}_1, \tilde{p}_2, \tilde{p}_3) = (-4, -3, 2)$. $r = \sum_j W_j^N \tilde{p}_j \pmod{Q}$;
 $\Sigma = -4W_1^N - 3W_2^N + 2W_3^N$.

Interestingly, Eq. (42) applies to any distinct flux switching routine regardless of the dwell times involved. This is illustrated in Tables I and II where the winding in

the first gap is different ($W^N = -2$ vs. $W^N = 0$) due to the different dwell times, but the underlying Diophantine equation used to label the gaps is still obeyed.

IV. DISCUSSION

In this work we studied the topology and gap organization of Floquet flux-switching drives via the Harper–Hofstadter model. Generically, for a periodic drive comprised of a series of fluxes $\{p_j/q_j\}$, the quasienergies are organized into $Q = \text{lcm}\{q_j\}$ magnetic subbands. For the simplest nontrivial case of the two-step $-1/2 \rightarrow 1/2$ flux drive with nonzero NNN hopping the bulk Floquet operator, $U(\mathbf{k}, T)$, can be interpreted as a single net $\text{SU}(2)$ rotation comprised of two distinct rotations with individual rotation angles proportional to the dwell times spent at $-1/2$, and $+1/2$ flux. We determined the Chern numbers for the upper and lower bands to be

$$C = \mp \text{sgn}[\sin(4t'(T_2 - T_1))],$$

valid whenever the 0 and π/T gaps are open, and where the upper and lower signs correspond to the top and bottom bands in the principal Floquet zone respectively. This formula captures the Chern inversion observed in our strip spectra and agrees with the numerically calculated RLBL windings in the regimes where $W_\pi = 2$.

The bulk Floquet operator for a general flux switching drive may be interpreted as a series of $\text{SU}(Q)$ rotations, where the culmination of all terms in a product gives one single equivalent rotation, $U(\mathbf{k}, T)$. The quasienergies for the general case were found to have a Wannier-like labeling structure via the adapted Floquet–Středa formula, Eq. (33). Namely, we found a Diophantine equation that relates gap labels in the quasienergy spectrum to the per-step “normal” windings explored during the periodic flux drive. The winding in any gap is partitioned into normal and anomalous contributions via $W = W^N + W^A$; the normal contribution and the fluxes of the drives are combined into a L -dimensional Diophantine equation for an L -step drive as

$$r \pmod{Q} = \sum_{j=1}^L W_j^N \tilde{p}_j \pmod{Q}, \quad (43)$$

where the total normal winding is the sum of the per-step winding $W^N = \sum_{j=1}^L W_j^N$, $\tilde{p}_j = Qp_j/q_j$, and the mod Q on the left hand side of the equality ensures the relation holds in the extended Floquet zone. Given this formulation, it is understood that the top and bottom gaps share $r = 0$. Notably, this expression is entirely agnostic to the frequency of the actual drive—it defines a congruence that must be followed for a given set of flux quenches, and thus it may be understood as a rule which dictates the allowed transfer of “normal” topological charge (not accounting for a changing W^A) across band touching events as dwell times are tuned. Hence, the set

of windings featured in the spectrum may be engineered in a predictable fashion by selecting a set of fluxes in a drive and tuning the respective dwell times. Because W^A is not featured in this expression the “rule-set” that dictates how W^A can change between driving periods is different—a subject for future investigation.

Future investigations should also consider time-reversal symmetric drives with spinful particles of the form $U(T) = U_{-\alpha_1}(T_1)U_{-\alpha_2}(T_2)\dots U_{\alpha_2}(T_2)U_{\alpha_1}(T_1)$ as these protocols are candidates for hosting nontrivial \mathbb{Z}_2 invariants which protect helical edge states. Furthermore, although non-magnetic weak disorder is not expected to destroy the topology of the bands in this drive (as it does not destroy the topology of the static Harper-Hofstadter bands), the effects of strong disorder and particle-particle interactions in the Bose-Hubbard or Fermi-Hubbard models are certainly interesting future directions to explore.

This research was generously supported by the William and Linda Frost Fund in the Cal Poly Bailey College of Science and Mathematics.

Appendix A: Ramping terms in the $-1/2 \rightarrow 1/2$ Flux-Switching Routine

To investigate the effect of explicitly including ramping terms in the $-1/2 \rightarrow 1/2$ switching routine we modify the ideal Floquet operator in Eq. (23) to be

$$U(\mathbf{k}, T) = U_d(\mathbf{k}, \tau)U_{+1/2}(\mathbf{k}, T_2)U_u(\mathbf{k}, \tau)U_{-1/2}(\mathbf{k}, T_1), \quad (\text{A1})$$

where the up and down ramp evolution operators are given as the time-ordered products

$$U_u(\mathbf{k}, \tau) = \prod_{j=1}^{N-1} U_j(\mathbf{k}, \delta\tau); \quad U_d(\mathbf{k}, \tau) = \prod_{j=1}^{N-1} U_{N-j}(\mathbf{k}, \delta\tau), \quad (\text{A2})$$

with the constituent unitaries defined as

$$U_j(\mathbf{k}, \delta\tau) = \exp[-iH_{-1/2+j/N}(\tau/N)] \quad (\text{A3})$$

and the corresponding Hamiltonians computed via Eq. (31) using the appropriate value of Q given the number of steps in the ramp. We plot the ramp-modified quasienergy spectrum for a ramping time of $\tau = 0.225$ in Fig. 5. Notably, the two primary quasienergy gaps survive the inclusion of the ramping unitaries.

Appendix B: $-\frac{1}{2} \rightarrow +\frac{1}{2}$ Flux-Switching Chern Numbers

For any two-level Hamiltonian $H(\mathbf{k}) = \mathbf{h}(\mathbf{k}) \cdot \boldsymbol{\sigma}$, the Chern number of one band can be obtained from the index formula [31]:

$$C = \frac{1}{2} \sum_{\mathbf{k}_\alpha \in \mathcal{D}_i} \text{sgn}[(\partial_{k_x} \mathbf{h} \times \partial_{k_y} \mathbf{h})_i] \text{sgn}(h_i(\mathbf{k}_\alpha)), \quad (\text{B1})$$

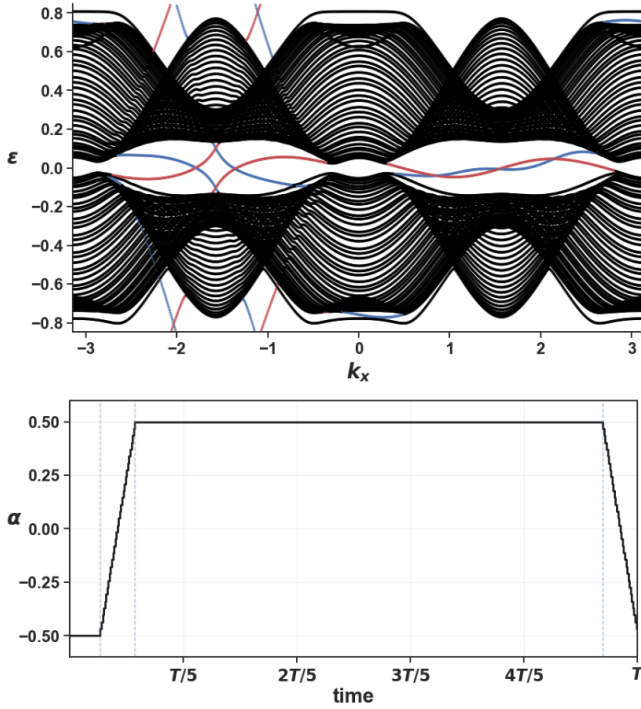


FIG. 5. $-1/2 \rightarrow 1/2$ flux switching quasienergy spectrum and ramping flux schedule with $T_1 = 0.2$, $T_2 = 3.05$, $t' = 0.3$, $t = 1$, and $\tau = 0.225$. Thirty terms at equally spaced distinct fluxes between $-\pi$ and π are scanned through each ramp. Gaps are closed when ramp times exceed $\tau \approx 0.35$.

where $i \in \{x, y, z\}$ is arbitrary and $\mathcal{D}_i = \{\mathbf{k} : h_j(\mathbf{k}) = h_\ell(\mathbf{k}) = 0\}$ with $\{i, j, \ell\} = \{x, y, z\}$.

For the two-step protocol $-\frac{1}{2} \rightarrow +\frac{1}{2}$ with dwell times T_1, T_2 , we have the following definitions

$$\mathbf{h}_\pm(\mathbf{k}) = (\cos k_y, \mp 2\tilde{t} \sin k_x \sin k_y, \cos k_x), \quad \tilde{t} = \frac{t'}{t},$$

$$|\mathbf{h}| = \sqrt{\cos^2 k_x + \cos^2 k_y + 4\tilde{t}^2 \sin^2 k_x \sin^2 k_y}.$$

The bulk Floquet operator is given as the product $U(\mathbf{k}, T) = U_+(\mathbf{k}, T_2) U_-(\mathbf{k}, T_1)$, where

$$U(\mathbf{k}, T) = e^{i\Theta(\mathbf{k}) \hat{\mathbf{n}}_F \cdot \boldsymbol{\sigma}}, \quad U_-(\mathbf{k}, T_1) = e^{i\theta_1(\mathbf{k}) \hat{\mathbf{n}}_- \cdot \boldsymbol{\sigma}},$$

$$U_+(\mathbf{k}) = e^{i\theta_2(\mathbf{k}) \hat{\mathbf{n}}_+ \cdot \boldsymbol{\sigma}}, \quad \theta_{1,2} = 2t T_{1,2} |\mathbf{h}|, \quad \hat{\mathbf{n}}_\pm = \frac{\mathbf{h}_\pm}{|\mathbf{h}|}.$$

From the standard SU(2) product rule,

$$\hat{\mathbf{n}}_F \sin \Theta = \hat{\mathbf{n}}_+ \sin \theta_1 \cos \theta_2 \quad (\text{B2})$$

$$+ \hat{\mathbf{n}}_- \sin \theta_2 \cos \theta_1 + (\hat{\mathbf{n}}_- \times \hat{\mathbf{n}}_+) \sin \theta_1 \sin \theta_2, \quad (\text{B3})$$

and noting $(\hat{\mathbf{n}}_- \times \hat{\mathbf{n}}_+)_y = 0$ here (only the y component flips between steps), the y -component reduces to

$$n_{F,y}(\mathbf{k}) \sin \Theta(\mathbf{k}) = \frac{2\tilde{t} \sin k_x \sin k_y}{|\mathbf{h}|} \sin(\theta_2(\mathbf{k}) - \theta_1(\mathbf{k})). \quad (\text{B4})$$

Choosing $i = y$ in (B1) and defining the flattened $\mathbf{h} = \hat{\mathbf{n}}_F$ we may proceed with the calculation of Eq. (B1) using the set $\mathcal{D}_y = \{\mathbf{k} : n_{F,x} = n_{F,z} = 0\}$

$$\mathcal{D}_y = \{\mathbf{k} : \cos k_x = 0, \cos k_y = 0\}. \quad (\text{B5})$$

Within the RBZ this corresponds to the two points

$$\mathbf{k}_\alpha \in \left\{ \left(+\frac{\pi}{2}, \frac{\pi}{2} \right), \left(-\frac{\pi}{2}, \frac{\pi}{2} \right) \right\}.$$

At these points $|\mathbf{h}(\mathbf{k}_\alpha)| = 2|\tilde{t}|$, hence

$$\theta_2(\mathbf{k}_\alpha) - \theta_1(\mathbf{k}_\alpha) = 2t(T_2 - T_1) |\mathbf{h}(\mathbf{k}_\alpha)| = 4 \text{sgn}(t) |t'| (T_2 - T_1).$$

From (B4), and choosing the branch with $\sin \Theta > 0$ we have

$$\text{sgn}(n_{F,y}(\mathbf{k}_\alpha)) = \text{sgn}(\tilde{t}) s_\alpha \text{sgn}(\sin(\theta_2 - \theta_1)), \quad (\text{B6})$$

where we have defined the shorthand

$$s_\alpha = \text{sgn}(\sin k_x^\alpha \sin k_y^\alpha) \in \{+1, -1\}.$$

A linearization of $(n_{F,x}, n_{F,z})$ around \mathbf{k}_α gives the local orientation factor

$$\text{sgn} \left[(\partial_{k_x} \hat{\mathbf{n}}_F \times \partial_{k_y} \hat{\mathbf{n}}_F)_y \right]_{\mathbf{k}_\alpha} = -s_\alpha, \quad (\text{B7})$$

so each point contributes with the same overall sign after multiplying (B6)–(B7).

Using (B1) with the flattened $\mathbf{h} = \hat{\mathbf{n}}_F$ and summing the two \mathbf{k}_α , we obtain the Chern number for the lower band of $\hat{\mathbf{n}}_F$

$$C_{\text{lower}} = -\text{sgn}(\tilde{t}) \text{sgn}(\sin(\theta_2 - \theta_1)).$$

The “bottom” Floquet band (negative quasienergy in the principal Floquet zone) corresponds to the $+$ eigenstate of $\hat{\mathbf{n}}_F$ via $U(\mathbf{k}, T) = e^{-iH_F T}$, so its Chern number is

$$C_b = -C_{\text{lower}} = \text{sgn}(\tilde{t}) \text{sgn}(\sin(\theta_2 - \theta_1)).$$

Evaluated at \mathbf{k}_α this yields

$$C_b = \text{sgn} \left(\sin \left[4t' (T_2 - T_1) \right] \right), \quad (\text{B8})$$

valid whenever the gaps at 0 and π/T are open.

[1] N. Goldman and J. Dalibard, Periodically driven quantum systems: effective hamiltonians and engineered gauge

fields, Phys. Rev. X **4**, 031027 (2014).

[2] T. Oka and S. Kitamura, Floquet engineering of quantum

- materials, *Annu. Rev. Condens. Matter Phys.* **10**, 387 (2019).
- [3] A. Eckardt, Colloquium: Atomic quantum gases in periodically driven optical lattices, *Rev. Mod. Phys.* **89**, 011004 (2017).
- [4] D. H. Dunlap and V. M. Kenkre, Dynamic localization of a charged particle moving under the influence of an electric field, *Phys. Rev. B* **34**, 3625 (1986).
- [5] F. Grossmann, T. Dittrich, P. Jung, and P. Hänggi, Coherent destruction of tunneling, *Phys. Rev. Lett.* **67**, 516–519 (1991).
- [6] T. Kitagawa, E. Berg, M. Rudner, and E. Demler, Topological characterization of periodically driven quantum systems, *Phys. Rev. B* **82**, 235114 (2010).
- [7] E. B. M. S. Rudner, N. H. Lindner and M. Levin, Anomalous edge states and the bulk-edge correspondence for periodically driven two-dimensional systems, *Phys. Rev. X* **3**, 031005 (2013).
- [8] F. Nathan, D. A. Abanin, E. Berg, N. H. Lindner, and M. S. Rudner, Anomalous floquet insulators, *Phys. Rev. B* **99**, 195133 (2019).
- [9] M. C. Rechtsman, J. M. Zeuner, Y. Plotnik, Y. Lumer, S. Nolte, M. Segev, and A. Szameit, Photonic floquet topological insulators, *Nature* **496**, 196 (2013).
- [10] G. Jotzu, M. Messer, R. Desbuquois, M. Lebrat, T. Uehlinger, D. Greif, and T. Esslinger, Experimental realization of the topological haldane model with ultracold fermions, *Nature* **515**, 237 (2014).
- [11] L. J. Maczewsky, J. M. Zeuner, S. Nolte, and A. Szameit, Observation of photonic anomalous floquet topological insulators, *Nature Communications* **8**, 13756 (2017).
- [12] J. W. McIver, B. Schulte, F.-U. Stein, T. Matsuyama, G. Jotzu, T. Meier, and A. Cavalleri, Light-induced anomalous hall effect in graphene, *Nature Physics* **16**, 38 (2020).
- [13] W. Zhu, H. Xue, J. Gong, Y. Chong, and B. Zhang, Time-periodic corner states from floquet higher-order topology, *Nature Communications* **13**, 11 (2022).
- [14] M. A. *et al.*, Realization of the hofstadter hamiltonian with ultracold atoms in optical lattices, *Phys. Rev. Lett.* **111**, 185301 (2013).
- [15] H. M. *et al.*, Realizing the harper hamiltonian with laser-assisted tunneling in optical lattices, *Phys. Rev. Lett.* **111**, 185302 (2013).
- [16] E. Brown, Bloch electrons in a uniform magnetic field, *Phys. Rev.* **133**, A1038 (1964).
- [17] J. Zak, Magnetic translation group, *Phys. Rev.* **134**, A1602 (1964).
- [18] J. Zak, Magnetic translation group ii. irreducible representations, *Phys. Rev.* **134**, A1607 (1964).
- [19] Y.-J. Lin, R. L. Compton, K. Jiménez-García, W. D. Phillips, J. V. Porto, and I. B. Spielman, A synthetic electric force acting on neutral atoms, *Nature Physics* **7**, 531 (2011).
- [20] D. A. Abanin, W. De Roeck, W. W. Ho, and F. Huveneers, Effective hamiltonians, prethermalization, and slow energy absorption in periodically driven many-body systems, *Phys. Rev. B* **95**, 014112 (2017), arXiv:1510.03405 [cond-mat.stat-mech].
- [21] D. J. Thouless, M. Kohmoto, M. P. Nightingale, and M. den Nijs, Quantized hall conductance in a two-dimensional periodic potential, *Physical Review Letters* **49**, 405 (1982).
- [22] D. Carpentier, P. Delplace, M. Fruchart, and K. Gawędzki, Topological index for periodically driven time-reversal invariant two-dimensional systems, *Physical Review Letters* **114**, 106806 (2015), arXiv:1503.04157 [cond-mat.mes-hall].
- [23] L. Peralta Gavensky, G. Usaj, and N. Goldman, The Středa Formula for Floquet Systems: Topological Invariants and Quantized Anomalies from Cesàro Summation 10.48550/arXiv.2408.13576 (2025), arXiv:2408.13576v3, arXiv:2408.13576 [cond-mat.mes-hall].
- [24] O. Morikawa and H. Suzuki, Winding number on 3d lattice, (2024), arXiv:2412.03888 [hep-lat].
- [25] P. Středa, Theory of quantised hall conductivity in two dimensions, *Journal of Physics C: Solid State Physics* **15**, L717 (1982).
- [26] F. Nathan and M. S. Rudner, Topological singularities and the general classification of floquet–bloch systems, *New Journal of Physics* **17**, 125014 (2015), arXiv:1506.07647 [cond-mat.mes-hall].
- [27] J. K. Asbóth and A. Alberti, Spectral flow and global topology of the hofstadter butterfly, *Physical Review Letters* **118**, 216801 (2017), arXiv:1611.07052 [cond-mat.mes-hall].
- [28] G. H. Wannier, A result not dependent on rationality for bloch electrons in a magnetic field, *Phys. Status Solidi B* **88**, 757 (1978).
- [29] G. Montambaux and M. Kohmoto, Quantized hall effect in three dimensions, *Phys. Rev. B* **41**, 11417 (1990).
- [30] M. Kohmoto, B. I. Halperin, and Y.-S. Wu, Diophantine equation for the three-dimensional quantum hall effect, *Phys. Rev. B* **45**, 13488 (1992).
- [31] D. Sticlet, F. Piéchon, J.-N. Fuchs, P. Kalugin, and P. Simon, Geometrical engineering of a two-band chern insulator in two dimensions with arbitrary topological index, *Physical Review B* **85**, 165456 (2012).